INFORMS Journal on Computing

Robust Optimization of Dose-Volume Metrics for Prostate HDR-Brachytherapy Incorporating Target and OAR Volume Delineation Uncertainties

Marleen Balvert, Dick den Hertog, Aswin L. Hoffmann,

Please scroll down for article—it is on subsequent pages

Robust Optimization of Dose-Volume Metrics for Prostate HDR-Brachytherapy Incorporating Target and OAR Volume Delineation Uncertainties

Marleen Balvert,[a, b, c] Dick den Hertog,[a] Aswin L. Hoffmann[d, e, f]

[a] Department of Econometrics and Operations Research/Center for Economic Research (CentER), Tilburg University, 5000 LE Tilburg, Netherlands; [b] Centrum voor Wiskunde en Informatica, 1098 XG Amsterdam, Netherlands; [c] Theoretical Biology and Bioinformatics, Utrecht University, 3508 TC Utrecht, Netherlands; [d] Institute of Radiooncology, Helmholtz-Zentrum Dresden-Rossendorf, Dresden, Germany; [e] Department of Radiotherapy and Radiooncology, University Hospital Carl Gustav Carus at the Technische Universität Dresden, Dresden, Germany; [f] Department of Radiation Oncology (MAASTRO), GROW School for Oncology and Developmental Biology, Maastricht University Medical Center, Maastricht, Netherlands

Contact: m.balvert@cwi.nl, http://orcid.org/0000-0002-2376-9301 (MB); d.denhertog@tilburguniversity.edu (DdH); aswin.hoffmann@oncoray.de (ALH)

Abstract. In radiation therapy planning, uncertainties in the definition of the target volume yield a risk of underdosing the tumor. The traditional corrective action in the context of external beam radiotherapy (EBRT) expands the clinical target volume (CTV) with an isotropic margin to obtain the planning target volume (PTV). However, the EBRT-based PTV concept is not directly applicable to brachytherapy (BT) since it can lead to undesirable dose escalation. Here, we present a treatment plan optimization model that uses worst-case robust optimization to account for delineation uncertainties in interstitial high-dose-rate BT of the prostate. A scenario-based method was developed that handles uncertainties in index sets. Heuristics were included to reduce the calculation times to acceptable proportions. The approach was extended to account for delineation uncertainties of an organ at risk (OAR) as well. The method was applied on data from prostate cancer patients and evaluated in terms of commonly used dosimetric performance criteria for the CTV and relevant OARs. The robust optimization approach was compared against the classical PTV margin concept and against a scenario-based CTV margin approach. The results show that the scenario-based margin and the robust optimization method are capable of reducing the risk of underdosage to the tumor. As expected, the scenario-based CTV margin approach leads to dose escalation within the target, whereas this can be prevented with the robust model. For cases where rectum sparing was a binding restriction, including uncertainties in rectum delineation in the planning model led to a reduced risk of a rectum overdose, and in some cases, to reduced target coverage.

1. Introduction

Cancer can be treated by surgery, chemotherapy, radiotherapy or a combination of these modalities. For deep-seated solid tumors, radiotherapy is an adequate treatment option as ionising radiation can penetrate healthy tissues to reach the tumor. Radiation therapy can be delivered by external beam radiotherapy (EBRT) or by brachytherapy (BT). Radiation in EBRT comes from an external source and is pointed at the tumor, while with BT a small radioactive source is placed inside or close to the tumor.

For prostate cancer, which is the most common type of cancer among men in the Western world, interstitial high-dose rate brachytherapy (HDR-BT) with a temporary implant has been shown to be an adequate treatment (Yamada et al. 2012). A template containing a large number of evenly spaced holes is typically placed in front of the patient's perineum while he is under anesthesia in dorsal position. Depending on the dimensions of the prostate, around 15 to 20 of these holes are selected for implanting a hollow catheter into the prostate. After implantation of all needles, a remote afterloader device successively advances a ^{192}Ir source through the needles. The source stops in each catheter at predetermined locations (dwell positions) inside the target volume for a predetermined amount of time

(dwell time) to deposit a sufficiently high dose to the tumor. The source is then removed from the patient and stored in the afterloader device for future use.

Radiotherapy inevitably results in exposure of healthy tissues surrounding the tumor. The spatial distribution of catheters and dwell positions, together with the dwell times, determine the shape and magnitude of the dose distribution. The goal of treatment planning is to determine the number and locations of catheters together with the dwell times such that the tumor receives a sufficiently high dose to sterilize the tumorous cells while limiting dose exposure to surrounding organs at risk (OARs) as much as possible to minimize the risk of side effects. The problem of designing a treatment plan for HDR-BT lends itself to be formulated as a mathematical optimization problem (De Boeck et al. 2014).

A scan of the patient's anatomy is made before treatment planning, and the target volume and the OARs are delineated (Figure 1). These delineations are subject to intra- and inter-observer variability, i.e., the same observer does not draw identical contours for the same individual case, and different observers produce different delineations for an identical case, respectively (see e.g., Villeirs et al. 2005 and De Brabandere et al. 2012). This implies uncertainty in the location and shape of the delineated structures, and thus uncertainty in the volumes to be irradiated and those to be spared. To numerically optimize and evaluate a dose distribution, these structures are discretized into finite sets of small volume elements that are considered dose calculation points. The dose deposited in each calculation point is the superposition of the dose rate contributions from

Figure 1. A Transrectal Ultrasound Image with Delineated Target Volume (Black) Extended with an Isotropic Margin (White), Rectum (Gray, Dashed), and Urethra (Gray, Solid)
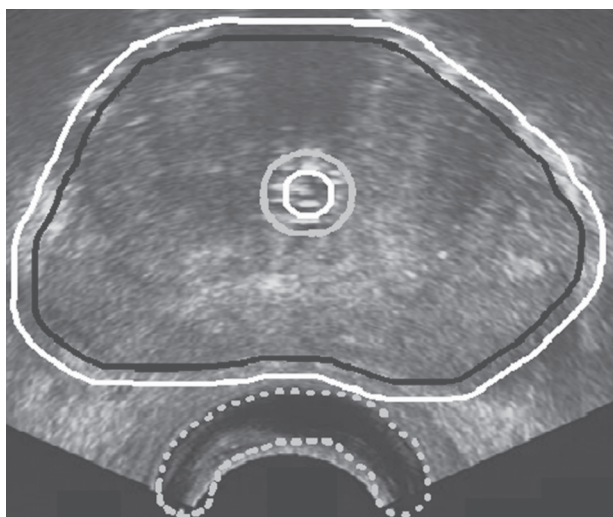
Note. The white delineation is a safety margin accounting for uncertainties, see Section 1.1.1.

Figure 2. Two Delineations of a Prostatic Target Volume Based on a Transversal Ultrasound Imaging Scan
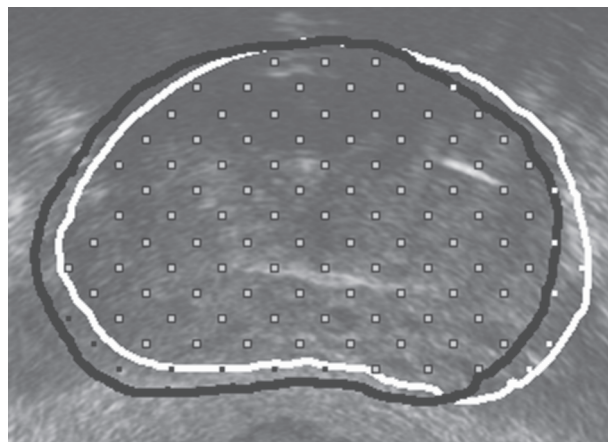
Note. Both delineations yield a different set of calculation points residing in the structure: The gray points with a black outline reside in both structures, the white and black points only in the white and black delineation, respectively.

all the dwell positions weighted by their respective dwell times. Hence, uncertainties in the delineations translate into uncertainty as to whether a calculation point belongs to a certain structure (Figure 2). This implies that there is uncertainty in the index sets of the optimization model. So far, to our knowledge, optimization methods have not addressed this type of uncertainty. Therefore, our aim here is to develop an optimization method that is robust against uncertainty in index sets, and that consequently can be applied for robust optimization of HDR-BT dose distributions incorporating delineation uncertainties.

1.1. Review of Methods Accounting for Uncertainties in Treatment Planning from Clinical Practice and Literature

The classical way to address geometrical uncertainties in EBRT planning is to apply a margin around the tumor volume such that a sufficiently large volume receives the prescribed therapeutic dose (e.g., Van Herk et al. 2002, Van Herk 2004). A more recent approach uses computational methods to numerically account for uncertainties during the treatment planning optimization process. Methods such as stochastic programming (e.g., Unkelbach and Ulfke 2004, Bohoslavsky et al. 2013) and worst-case robust optimization (e.g., Chan et al. 2006, Bortfeld et al. 2008, Fredriksson 2013) have been suggested for this task.

1.1.1. Margin Approach. According to international consensus guidelines published in the ICRU 62 report (International Commission on Radiation Units and Measurements 1999), uncertainties in EBRT should be accounted for by applying a margin around the tumor volume. Treatment preparation starts by delineating the gross palpable, visible or clinically demonstrable

location of the tumor on a scan, yielding the gross tumor volume (GTV). Because microscopic disease spread surrounding the GTV is invisible on the scan, the GTV is expanded with a certain margin, resulting in the clinical target volume (CTV). An additional margin is applied to account for geometrical uncertainties in treatment planning (e.g., errors due to organ filling and movement) and delivery (e.g., set-up errors due to patient and beam positioning), which results in the planning target volume (PTV).

The PTV concept as described in the ICRU 62 report has been developed for EBRT, where the aim is to expand the dose distribution into a homogeneous plateau reaching beyond the CTV. However, for BT (Tanderup et al. 2010, p. 499) noted that "a homogeneous dose cannot be obtained in and around a brachytherapy CTV," since adding PTV margins would lead to an undesirable dose escalation within the target. Applying a margin around the CTV to account for delineation uncertainties is thus not applicable for BT. Nevertheless, the margin recipe is currently used in BT practice.

1.1.2. Robust Optimization. So far, robust optimization and stochastic programming have only been applied to treatment planning models for EBRT. Stochastic programming considers the probability distribution of an uncertain parameter, for example through optimizing the expectation of the objective function or by restricting the probability of constraint violations (e.g., Chu et al. 2005, Olafsson and Wright 2006, Unkelbach and Ulfke 2004, Bohoslavsky et al. 2013, Fredriksson 2013). This inherently requires knowledge or assumptions about the probability distribution of the uncertain parameter. However, such information is typically unavailable, which is the case in our application. Worst-case robust optimization instead assumes an uncertainty region or a scenario-set in which the uncertain parameter resides. A worst-case robust optimization model only considers solutions that are robust feasible, i.e., solutions that are feasible for all possible realizations of the parameters. Among these solutions, a worst-case robust optimization problem selects the solution that minimizes (maximizes) the maximum (minimum) over all possible parameter values or scenarios of the objective function (Ben-Tal et al. 2009). Worst-case robust optimization thus yields treatment plans that perform better in the worst-case scenario (Fredriksson 2012). Robust optimization for EBRT has been considered by various groups and can be applied to treatment planning models at three different levels: One can require robustness per calculation point (e.g., Chan et al. 2006, Bortfeld et al. 2008, Liu et al. 2012), per objective and constraint (Chen et al. 2011) or for the complete model (e.g., Fredriksson et al. 2011). For a detailed comparison of these three approaches for proton therapy planning, see Fredriksson and

Bokrantz (2014). In our opinion, each constraint should be satisfied in all of the scenarios, and the robustness of each objective should be considered separately (as opposed to an aggregate of the objectives). We have a single objective and several planning constraints in our model, and we apply robust optimization to each objective and constraint.

The methods described above have been applied to EBRT planning models for various types of uncertainties (e.g., organ motion or set-up uncertainties), but, to our knowledge, none have considered delineation uncertainties. However, uncertainties in target volume delineation are known to be among the major causes of geometrical uncertainties (Weiss and Hess 2003) in EBRT and BT. The importance of accounting for any type of uncertainty in BT planning models has been emphasized by Kirisits et al. (2014). In particular, they note that intra- and inter-observer delineation variabilities, together with intra- and inter-fraction set-up uncertainties, contribute most to dosimetric uncertainty. Also, Rylander et al. (2017) found that delineation uncertainties can lead to a degradation of dose. To our knowledge, methods for robust treatment planning have so far only considered uncertainties that yield uncertainty in the location of the calculation point relative to the radiation source (e.g., through organ motion or set-up uncertainties), while the structure to which the calculation point belongs is fixed. This implies uncertainty in the dose rate (i.e., the dose per unit time), which is an important input parameter in treatment planning optimization models. On the other hand, delineation uncertainties do not change the location of a calculation point, so the dose rate remains fixed. Instead, they yield uncertainty in the structure to which a calculation point belongs. To our knowledge, the literature on robust optimization only considers uncertainty in input parameters. As our problem concerns uncertainty in index sets, we cannot use previously developed models: a new approach is required.

1.2. Aim and Contribution of the Paper
Our goal here is to take delineation uncertainties into account in the treatment planning optimization process for prostate HDR-BT using a worst-case robust optimization approach. We develop a worst-case robust optimization method to incorporate uncertainties in index sets. We aim to reduce the risk of underdosing the CTV while respecting the predefined OAR constraints. We compare our method to the classical margin approach.

The contributions of this work are (1) using computational methods to incorporate delineation uncertainties in treatment plan optimization, (2) extending the robust optimization approach to account for uncertainties in index sets, (3) using robust optimization to

address uncertainties in BT, and (4) providing a speed-up for the nominal BT treatment planning model that optimizes clinical objectives (Gorissen et al. 2013).

This paper is organized as follows. In Section 2, HDR-BT plan optimization is further clarified (Section 2.1) and the nominal model for HDR-BT of prostate cancer is introduced (Section 2.2). In Section 2.3 three methods to address delineation uncertainties are discussed. An extension of the model to account for rectum delineation uncertainties is presented in Section 2.4, and methods for reducing the calculation times are presented in Section 2.5. The computational experiments and their results, along with a comparison of the three approaches, are presented in Section 3. A discussion and conclusion are provided in Sections 4 and 5, respectively.

2. Treatment Plan Optimization Model
2.1. Dose Prescription and Plan Evaluation

The dosimetric quality of a treatment plan is usually evaluated using dose-volume histograms (DVHs). These metrics are denoted by $D_{x\%}(S)$ and $D_{xcc}(S)$, which reflect the minimum dose received by the hottest $x\%$ and x cc of the structure volume S, respectively, or by $V_{y\%}(S)$ and $V_{yGy}(S)$, which denotes the fraction of the structure volume S receiving at least $y\%$ of the prescribed tumor dose or y Gy. A treatment plan should satisfy pre-set DVH constraints. An example of a dose prescription protocol for prostate HDR-BT, for which the rectum and urethra are the most relevant OARs, is presented in Table 1. Here, $D_{90\%}(PTV)$ is given as a percentage of the prescribed tumor dose. Note that uncertainties are accounted for using a CTV-to-PTV margin and that dose prescriptions are defined for the PTV and not for the CTV. The same prescriptions are used for the PTV in clinical practice; we also use them to assess plan quality.

2.2. Nominal Treatment Planning Model

The optimization models currently used by treatment planning systems assign a penalty to each calculation point based on the difference between the planned and the prescribed dose, and they minimize the total penalty (e.g., Lessard and Pouliot 2001). Because such penalties are a surrogate for the actual planning goals, which is to satisfy the pre-set DVH criteria, recently

Table 1. Dose-Volume Criteria Based on the Protocol by Hoskin et al. (2007)

PTV (%)	Rectum (Gy)	Urethra (Gy)
$D_{90\%} \geq 100$	$D_{10\%} \leq 7.2$	$D_{10\%} \leq 10$
$V_{100\%} \geq 95$	$D_{2cc} \leq 6.7$	$D_{0.1cc} \leq 10$
$V_{150\%} \leq 55$	$D_{max} \leq 8$	$D_{max} \leq 10.6$
$V_{200\%} \leq 20$		

developed methods directly optimize the DVH metrics (Siauw et al. 2011, Gorissen et al. 2013, Holm et al. 2013). We use the model from Gorissen et al. (2013).

Catheter locations and dwell time distributions are optimized in Gorissen et al. (2013), where active dwell locations are given for each candidate catheter location with a 3 mm separation. The goal is to maximize the fraction of the target volume receiving at least the prescribed dose, denoted by $V_{100\%}(CTV)$. The following model is referred to as the linear dose-volume, or (LDV):

$$(LDV) \quad \max \quad \frac{1}{|I_C|} \sum_{i \in I_C} v_i$$

$$\text{s.t.} \quad \dot{d}_i^T t \geq v_i D_{pres} \quad \forall i \in I_C \tag{1}$$

$$\dot{d}_i^T t \leq L_R + (H_R - L_R)(1 - w_i), \quad \forall i \in I_R \tag{2}$$

$$\sum_{i \in I_R} w_i \geq \tau_R |I_R| \tag{3}$$

$$t \geq 0$$

$$v_i \in \{0,1\} \quad \forall i \in I_C$$

$$w_i \in \{0,1\} \quad \forall i \in I_R$$

[see Section 1 in the online supplement for additional constraints].

Here, $\dot{d}_i \in \mathbb{R}_+^{|J|}$ is the vector with dose rates from each dwell position to calculation point i; I_C denotes the set of dose calculation points in the CTV, and J denotes the set of dwell positions. The optimization variable $t \in \mathbb{R}_+^{|J|}$ contains the (nonnegative) dwell times of all dwell positions. As a result, $\dot{d}_i^T t$ is the total dose planned to be delivered to calculation point i. D_{pres} is the prescribed dose to the PTV, and v_i is an auxiliary variable that equals 1 if calculation point i receives at least the prescribed dose, and 0 otherwise. The objective maximizes the fraction of calculation points receiving at least the prescribed dose. Constraint (2) ensures that no calculation point in the rectum receives a dose above H_R. The variable w_i equals 1 if calculation point i receives a dose below L_R, and 0 otherwise. Constraints (2) and (3) together restrict the fraction of calculation points in the rectum receiving a dose above L_R to be at most τ_R.

Additional constraints are included to restrict the dose to the urethra and to choose the number of catheters and their locations (see Section 1 of the online supplement). These constraints are not provided in detail here, as they remain the same in the robust model.

2.3. Accounting for Delineation Uncertainties of the PTV

We compare three approaches to incorporate delineation uncertainties in the plan optimization. These approaches are an isotropic CTV-to-PTV margin currently used in the clinic, a scenario-based CTV-to-PTV margin, and a robust optimization approach.

2.3.1. Isotropic CTV-to-PTV Margin. Despite the fact that a CTV-to-PTV margin seems unsuitable for HDR BT, such a tactic is currently used in the clinic to account for delineation uncertainties. As we compare our robust approach to the current clinical standard, we consider the isotropic CTV-to-PTV margin that replaces the set I_C by I_P in model (LDV), the latter of which is the set of calculation points in the PTV. An isotropic margin of 2 mm is used in (Hoskin et al. 2013).

2.3.2. Scenario-Based CTV-to-PTV Margin. Given a nominal delineation of the CTV and using measurements on delineation inaccuracies from Smith et al. (2007), we generate scenarios for possible delineations and the corresponding sets of CTV calculation points. Because the CTV-to-PTV margin is smaller than the delineation uncertainty reported in the literature, the PTV does not fully contain all the CTV scenarios, and I_P does not contain all of the calculation points that are in the CTV according to at least one scenario. Therefore, we also test the use of a scenario-based margin. The union of all CTV scenarios is considered as the PTV. The set of all calculation points that may be in the CTV according to our scenario set, denoted by $\tilde{I}_C$, is used instead of the set I_C in (LDV).

2.3.3. Robust Optimization. We use a scenario-based approach for our robust optimization model. We know the set of calculation points within the CTV for each scenario in the set S. This information is stored in matrix C, a $|S| \times |I|$ matrix, where each row corresponds to a scenario and each column corresponds to a calculation point. The entry on the sth row in the ith column equals 1 if calculation point i resides in the CTV for scenario s, and 0 otherwise. This matrix is used to calculate CTV coverage for each scenario s as $V_{100\%}^s(\text{CTV}) = C_s v / C_s e$, where C_s denotes row s of matrix C, e is the all-ones vector, and v is as before. The numerator counts the number of calculation points that receive at least the prescribed dose and are in the CTV according to scenario s, while the denominator counts the number of calculation points in the CTV according to scenario s.

The robust counterpart of the (LDV) model is

(RC) max V

$$\text{s.t. } V \leq \frac{C_s v}{C_s e} \quad \forall s \in S \tag{4}$$

$$\dot{d}_i^T t \geq D_{\text{pres}} v_i \quad \forall i \in \tilde{I}_C \tag{5}$$

$$t \geq 0$$

$$v_i \in \{0,1\} \quad \forall i \in \tilde{I}_C \tag{6}$$

$$\dot{d}_i^T t \leq L_R + (H_R - L_R)(1 - w_i) \quad \forall i \in I_R$$

$$\sum_{i \in I_R} w_i \geq \tau_R |I_R|$$

$$w_i \in \{0,1\} \quad \forall i \in I_R$$

[additional constraints are in the
     See Section 1 in the online supplement].

Initial tests show that (RC) yields a risk of overdosage, reflected by $V_{200\%}(\text{CTV})$ exceeding the desired maximum level as shown in Table 1. Therefore, we added the following constraints to (RC) to limit $V_{200\%}$ for each scenario:

$$\dot{d}_i^T t \leq 2D_{\text{pres}} + M u_i \quad \forall i \in \tilde{I}_C$$

$$\frac{C_s u}{C_s e} \leq 0.2 \quad \forall s \in S \tag{7}$$

$$u_i \in \{0,1\} \quad \forall i \in \tilde{I}_C,$$

where u_i is a binary variable that is 0 only if calculation point i receives at most twice the prescription dose and 1 otherwise, and M is an arbitrary large number. We have for scenario s that $V_{200\%}^s(\text{CTV}) = C_s u / C_s e$, which is restricted to be at most 0.2 according to the protocol by Hoskin et al. (2007); see Table 1.

The number of variables and constraints in (LDV) and (RC) are shown in Table 2, where we only consider the constraints and variables related to the target volume and skip the constraints and variables corresponding to OAR, sparing maximum dwell times and catheter choice, as these are identical for both models. This table clearly shows the major advantage of our approach: The number of binary variables does not increase with the number of scenarios $|S|$, but only with the number of calculation points in the uncertainty region $|\tilde{I}_C|$. The number of constraints increases linearly with $|S|$.

2.4. Accounting for Uncertainties in Rectum Delineation

To our knowledge, delineation uncertainties in the OARs are unaccounted for in clinical practice. The delineation of the urethra is rather accurate, as a Foley catheter is usually inserted that is well visible on images acquired before treatment planning. There is, however, variability in the rectal wall thickness. Indeed, the posterior rectal wall is invisible and not delineated when using transrectal ultrasound imaging. However, this volume receives little or no dose and is irrelevant. Delineation uncertainties in the cranial and caudal, as well as the lateral direction of the rectum, are also irrelevant, as these areas receive hardly any dose. Therefore, we only consider variabilities in delineating the anterior rectal wall.

Variabilities in delineation of the rectum can be accounted for using a margin or following a robust optimization approach. We consider the scenario-based margin.

Table 2. Problem Sizes for (LDV) and (RC)

	(LDV)	(RC)
No. of binary variables	$|I_P|$	$2|\tilde{I}_C|$
No. of continuous variables	$|J|$	$|J|$
No. of constraints	$|I_P|$	$2|S| + 2|\tilde{I}_C|$

For the robust optimization approach, we derive the robust counterpart of constraints (2) and (3). Following the same approach as for the PTV, we consider a set of scenarios for the delineation of the rectum. The rows of the matrix R correspond to the calculation points, and the columns correspond to the scenarios. An element R_{is} equals 1 if calculation point i is in the rectum according to scenario s, and 0 otherwise. We obtain the following robust counterpart of constraints (2) and (3):

$$\dot{d}_i^T t \leq L_R + (H_R - L_R)(1 - w_i) \quad \forall\, i \in \tilde{I}_R \qquad (8)$$
$$\frac{R_s^T w}{R_s^T e} \geq \tau_R,$$

where $\tilde{I}_R$ is the set containing all calculation points in the rectum according to at least one scenario.

It could be that the sets $\tilde{I}_C$ and $\tilde{I}_R$ overlap in space. However, as a different set of calculation points is generated for each structure, it is not possible that one calculation point belongs to two structures for some scenarios, and hence that two different restrictions are imposed for a single calculation point. This allows us to separately consider the worst case for the objective function and each constraint.

2.5. Reduction of Solution Times

Even though the number of binary variables increases only with the size of the uncertainty region, the solution time becomes more than several days, which is too long for the model to be used in practice, or may not be solved at all due to memory issues. We combine several heuristics to speed up the optimization. The algorithm is summarized in Figure 3.

First, we relax the requirement $v_i \in \{0, 1\}$ to $v_i \in [0, 1]$ for the CTV. Besides strongly reducing the number of binary variables and thus the calculation times, this relaxation has an appealing interpretation. For the binary variables and the continuous relaxation we have that $v_i = 1$ when calculation point i receives at least the prescribed dose. When i receives a dose below the prescription dose, the binary v_i equals 0, whereas the continuous variable v_i equals the delivered dose as a fraction of the prescribed dose. Thus, the dose to calculation point i is still pushed upward in the relaxation.

Second, optimization speed is improved by exploiting the fact that calculation points close to the catheters are likely to receive a high dose, while calculation points at a farther distance are likely to receive a low dose (see Nath et al. 1995). So, it may not be necessary to optimize for all calculation points in $\tilde{I}_C$. We initially assume that the calculation points near the catheters, denoted by the set $\tilde{I}_C^n$, receive at least the prescribed dose (i.e., $v_i = 1 \,\forall\, i \in \tilde{I}_C^n$), and that calculation points far from the catheters, denoted by $\tilde{I}_C^f$, do not

Figure 3. Flow Chart of the Algorithm Used to Solve (*RC*)
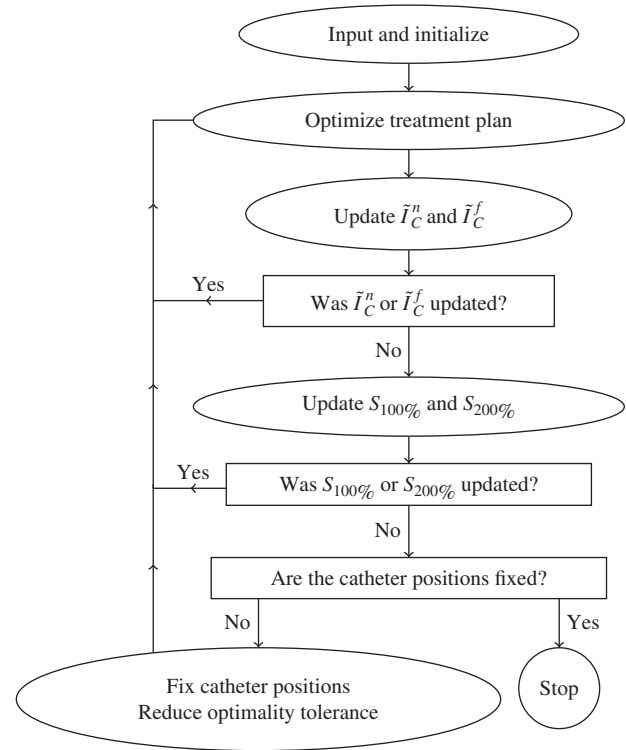
Note. Details of the procedures "Input and initialize," "Update $\tilde{I}_C^n$ and $\tilde{I}_C^f$," and "Update $S_{100\%}$ and $S_{200\%}$" are in Section 2 of the online supplement.

receive more than $2D_{\text{pres}}$ (i.e., $u_i = 1 \,\forall\, i \in \tilde{I}_C^f$). An example of such sets is illustrated in Figure 4. One could define these sets based on, e.g., the distance to the nearest dwell position. We define these sets based on the outcome of the nominal optimization model: All calculation points that receive a dose above D_{pres} or below $2D_{\text{pres}}$ when applying the nominal treatment plan optimized with (*LDV*) are included in $\tilde{I}_C^n$ and $\tilde{I}_C^f$, respectively. Note that no assumptions on the dose levels received are made for the calculation points outside $\tilde{I}_C^n$ and $\tilde{I}_C^f$. (*RC*) is optimized where constraints (4) and (7) only apply to calculation points in $\tilde{I}_C \backslash \tilde{I}_C^n$ and $\tilde{I}_C \backslash \tilde{I}_C^f$, respectively. We check each of the calculation points in

Figure 4. Example of Sets of Calculation Points That Are Likely to Receive a High ($\tilde{I}_C^n$) or a Low Dose ($\tilde{I}_C^f$)
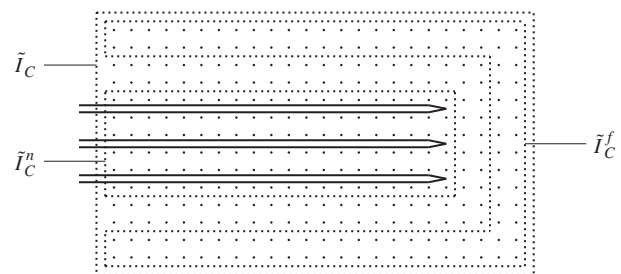
$\tilde{I}_C^n$ and $\tilde{I}_C^f$ to see if they receive a sufficiently high and low dose. If not, we exclude a predetermined number of the coldest and hottest calculation points from the sets $\tilde{I}_C^n$ and $\tilde{I}_C^f$, respectively, and re-optimize using the previous optimal treatment plan as a starting solution. We excluded $\eta_{100\%}|\tilde{I}_C|$ and $\eta_{200\%}|\tilde{I}_C|$ calculation points per iteration from the sets $\tilde{I}_C^n$ and $\tilde{I}_C^f$ in our experiments, where $\eta_{100\%}$, $\eta_{200\%} \in [0,1]$. This process is continued until the number of calculation points for which we made an incorrect assumption is sufficiently low (see Figure 3, and Section 2 of the online supplement).

Third, we implement the adversarial approach (Bienstock and Özbay 2008), which implies that only a subset of the scenarios is included in the optimization. We define two sets, $S_{100\%} \subset S$ and $S_{200\%} \subset S$. The first, $S_{100\%}$, contains those scenarios that determine the worst case $V_{100\%}$ in the objective, while the second, $S_{200\%}$, contains those scenarios for which we require $V_{200\%} \leq 0.2$. The robust model is thus solved with S replaced by $S_{100\%}$ in the $V_{100\%}$ objective and S replaced by $S_{200\%}$ for the constraint on $V_{200\%}$ of the CTV. This means that the resulting optimal solution is robust with respect to the scenarios in $S_{100\%}$, and $V_{200\%} \leq 0.2$ for the scenarios in $S_{200\%}$. Using the optimal treatment plan, the scenario with the lowest $V_{100\%}$(CTV) is added to $S_{100\%}$, unless it is already in the set. Furthermore, if the highest $V_{200\%}$ over all scenarios is larger than 0.2, the corresponding scenario is added to $S_{200\%}$. The new model instance is solved using the previous optimal solution as a starting point. The scenario sets are updated until no scenarios are added to either of the sets. Initially, $S_{100\%}$ only contains the nominal scenario and $S_{200\%}$ is empty (see Figure 3, and Section 2 of the online supplement).

The final iterations in the optimization are often spent on improving the optimality bound while the objective value largely plateaus. Furthermore, improving the objective a little may, in practice, have little effect on the dose to the tumor or OARs. It is thus unnecessary to solve the model to optimality. This particularly holds for optimization of the catheter configuration: The minor improvements in the final iterations are likely to result from a change in dwell times, not from a change in catheter configuration. We therefore optimize the robust model up to a pre-determined optimality gap g_1, fix the catheter configuration, and

continue optimizing the beam-on times up to a second, smaller optimality gap g_2 (see Figure 3).

3. Computational Experiments
3.1. Patient and Source Data
We use data from six prostate cancer patients to test our robust optimization method. The data is included as a supplement to this paper. Delineations of the CTV, rectum, and urethra were obtained from the treatment planning system, see Table 3 for the structure volumes. Data from patients 1, 2, and 3 were obtained from the planning system HDRplus (Eckert and Ziegler BEBIG GmbH, Berlin, Germany) and have previously been used in Gorissen et al. (2013) and Balvert et al. (2015). The delineations were originally made on images obtained with transrectal ultrasound. For these three patients, catheter and dwell locations could be obtained from the treatment planning system as well. Data from patients 4, 5, and 6 were obtained from Oncentra Brachy (Nucletron, Veenendaal, Netherlands), and were previously used in Deist and Gorissen (2016). The images of these patients were made using computed tomography. No data on catheter locations and dwell positions were available from the planning system and were therefore added by virtually placing a template in front of the perineum using MATLAB Release 2012b (MathWorks, Inc., Natick, Massachusetts).

Calculation points for all patients were hexagonally distributed over the structures using MATLAB Release 2012b (MathWorks, Inc., Natick, MA), see Table 4 for details. We used the same number of dose calculation points for optimization as did the treatment planning system; we used a larger set for the dosimetric evaluation of the treatment plan to obtain more accurate DVH measures. As the first three patients were imaged with transrectal ultrasound, only the anterior rectum wall was delineated, while for patients 4, 5, and 6 the complete rectum volume was delineated on the computed tomography scans. As the density of the calculation points was the same for all patients, the set of rectum calculation points is larger for patients 4, 5, and 6 than for the first three patients.

Dose rates were calculated according to the TG-43 formalism (Nath et al. 1995), for which

Table 3. Tissue Structure Volumes (cc)

Structure	Patient 1	Patient 2	Patient 3	Patient 4	Patient 5	Patient 6
Nominal CTV	31.7	55.2	47.6	31.0	40.1	32.7
Isotropic margin PTV	39.6	62.8	63.2	37.0	43.8	37.4
Scenario-based PTV	54.5	97.3	70.8	57.4	57.6	59.9
Nominal rectum	6.8	7.5	9.4	19.5	20.7	16.3
Scenario-based rectum	8.5	8.8	12.4	20.3	20.2	16.5
Urethra	2.1	2.6	2.3	1.3	3.0	1.3

Table 4. Number of Dose Calculation Points

Structure (set of cps)	Optimization					
	Pt 1	Pt 2	Pt 3	Pt 4	Pt 5	Pt 6
Nominal CTV (I_C)	1,750	1,759	1,743	1,757	1,749	1,743
Isotropic margin PTV (I_P)	1,777	1,754	1,757	1,790	1,772	1,795
Scenario-based PTV ($\tilde{I}_C$)	2,959	2,766	2,729	3,322	3,228	3,109
Nominal rectum (I_R)	249	253	251	257	259	256
Scenario-based rectum ($\tilde{I}_R$)	312	298	333	268	265	259
Urethra (I_U)	465	489	488	479	482	465
	Evaluation					
Nominal CTV (I_C)	8,108	8,112	8,246	8,676	8,166	8,058
Isotropic margin PTV (I_P)	7,955	7,892	8,423	8,214	8,273	8,133
Scenario-based PTV ($\tilde{I}_C$)	20,790	23,393	26,654	15,951	14,441	15,365
Nominal rectum (I_R)	2,586	2,533	2,542	6,252	6,283	6,124
Scenario-based rectum ($\tilde{I}_R$)	3,205	3,359	3,450	6,552	6,441	6,625
Urethra (I_U)	2,114	2,163	2,314	1,992	2,090	1,956

Note. Pt = Patient, cps = Calculation points.

[192]Ir source-specific parameters were obtained from Granero et al. (2006). The number of possible catheter positions and corresponding dwell positions are shown in Table 5.

3.2. Experimental Set-up

We defined the uncertainty region for the CTV with scenarios obtained from the original contours by stretching or shrinking the delineated target volume in the left, right, anterior, posterior, superior, and inferior direction. The centroid-to-surface distances in each direction were varied independently of each other. Distances were assumed to vary at most two standard deviations from the mean (delineated) distance. Standard deviations were obtained from Smith et al. (2007). For patients 1, 2, and 3, with whom transrectal ultrasound imaging was used, the standard deviations were 2.2 mm for the superior and inferior directions, and 1.15 mm for the remaining directions. Patients 4, 5, and 6 were imaged using computed tomography; their standard deviations were 1.15 mm in the cranial and caudal directions, 1.7 mm in the lateral directions, and 1.6 mm and 2 mm in the anterior and posterior directions, respectively. For patient 2, the original, smallest, and largest possible CTV shapes are depicted in Figure 5.

An uncertainty region for the rectum delineation was constructed through scenario generation as well.

Table 5. Number of Catheters and Dwell Positions

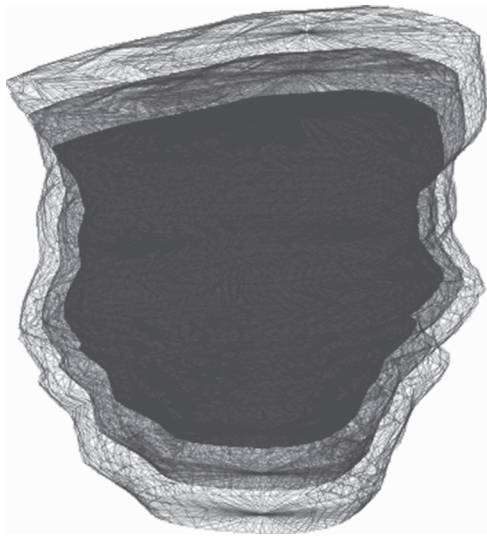|	Pt 1	Pt 2	Pt 3	Pt 4	Pt 5	Pt 6
Catheters	40	49	43	51	51	71
Dwell positions, original set	369	711	716	414	454	481
Dwell positions, extended set	432	813	836	657	582	653

Note. Pt = Patient, cps = Calculation points.

However, only variations in the anterior direction are of interest for the rectum, as this is where the highest dose is deposited. As a result, only three scenarios are included in the optimization: the smallest, the nominal, and the largest possible delineation. The smallest (largest) scenario was generated by shrinking (stretching) the rectum volume in the anterior direction by two standard deviations. We assume a standard deviation of 0.5 mm.

This method of scenario generation is straightforward as it neglects the fact that delineations of an observer may deviate from those delineated by others in a consistent manner; for example, one observer may always draw larger shapes than his/her colleague. The assumption of independent deviations in each direction may thus be invalid. However, to our knowledge, there is no data available on this dependency. Our method can be easily adapted if such data becomes available.

We considered only the minimum, nominal, and maximum distance for each direction to limit the number of scenarios taken into account in the optimization process, which gives $3^6 = 729$ possible shapes. Note that the assumption of independent deviations for each direction may result in unrealistically large or small shapes, e.g., when we fully stretch the shape in each direction, clinically, the volume becomes unrealistically large. Therefore, all scenarios with a clinically unrealistic CTV volume (smaller than 20 cc or larger than 65 cc) were excluded before optimization. This results in 596, 534, 602, 666, 729, and 729 scenarios for the six respective patients. To evaluate the plan quality, over 5,000 CTV scenarios were generated for each patient by randomly drawing centroid-to-surface distances for each direction. Again, extremely small and large scenarios were excluded. Recall that for the rectum only the uncertainty in the anterior rectal wall is relevant,

Figure 5. Vectorized Figure of Minimal (Dark Gray), Delineated (Medium Gray), and Maximum (Light Gray) CTV Shape

Figure 6. Sagittal Transrectal Ultrasound Scan with the PTV Delineated in Gray

Note. The black dwell positions are included in the original data set; the white ones are added to obtain the extended set of dwell positions.

which allows us to generate scenarios by stretching or shrinking the rectum in the anterior direction only. We generated 101 scenarios for which the factors by which the rectum was shrunk or stretched were sampled at equal distances on the interval from the minimum to the maximum possible deviation.

Models were compared based on DVH evaluation criteria for all scenarios as well as solution times. The models were solved using the Gurobi 5.5 optimizer (Gurobi Optimization, Inc., Houston, Texas) interfaced with MATLAB Release 2012b on a computer with an Intel i7-2670 QM processor.

The dwell positions that correspond to each catheter location are predefined by the planning software. Only the dwell positions in the PTV were activated and included in the optimization process. As the union of the CTV scenarios is larger than the original target volume, some dwell positions were excluded from the optimization process although they may be inside the target volume. It may thus be necessary to include additional dwell positions for each catheter. This is illustrated in Figure 6, where the PTV is delineated in white. The red dwell positions are included in the original data set, which can be extended by including the white dwell positions. All models are solved once using the original and once using the extended set of dwell positions.

A total of 10 treatment plans are optimized for each patient. The different optimization approaches are denoted by a three-letter code. The first letter denotes the approach taken to account for uncertainties in the delineation of the CTV, where I denotes the use of an isotropic CTV-to-PTV margin, S denotes the scenario-based margin, and the robust optimization approach is denoted by R. The second letter indicates the approach
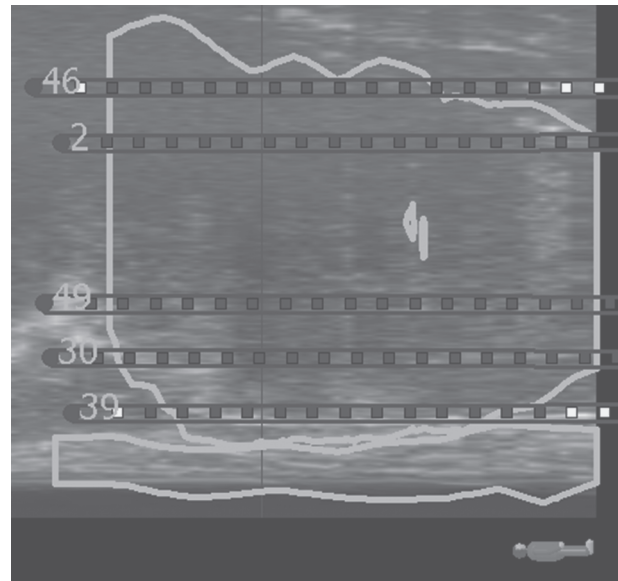
used to account for delineation uncertainties of the rectum, where N denotes the use of the nominal rectum delineation, and S and R are as before. Finally, the third letter indicates whether the original (O) or the extended (E) set of dwell positions is used. For example, INO denotes the optimization approach followed in the clinic, where an isotropic CTV-to-PTV margin is used, the nominal delineation is included for the rectum (so rectum delineation uncertainty is ignored), and the original set of dwell positions is used. An overview of the various settings used for the five optimization approaches is shown in Table 6.

The optimality gap g_2 is chosen as the smallest value for which the algorithm terminates within 15 minutes (a clinically acceptable optimization time) when optimizing RNO. This value differs per patient and can only be found through a trial-and-error search. The optimality gaps are shown in Table 7. Note that for patient 2 the optimality gap had to be adapted for the margin approach, as the optimizer ran out of memory for smaller values for g_2. The parameter g_1 is twice g_2. Parameters $\eta_{100\%}$ and $\eta_{200\%}$, the fractions of calculation points added to the sets $\tilde{I}_C^n$ and $\tilde{I}_C^f$ in each iteration, respectively, were 0.10.

3.3. Numerical Results

We first look at the effects of using continuous instead of binary variables v by comparing the results obtained with (LDV) to results obtained with its relaxation (Section 3.3.1). In Section 3.3.2, we compare the proposed methods to account for delineation uncertainties.

Table 6. Overview of the Settings Used for Each Optimization Approach

| | Method to account for uncertainties: | | |
	in CTV	in rectum	Dwell positions
INO	Isotropic margin	None	Original set
RNO	Worst case robust	None	Original set
RRO	Worst case robust	Worst case robust	Original set
SNO	Scenario-based margin	None	Original set
SSO	Scenario-based margin	Scenario-based margin	Original set
INE	Isotropic margin	None	Extended set
RNE	Worst case robust	None	Extended set
RRE	Worst case robust	Worst case robust	Extended set
SNE	Scenario-based margin	None	Extended set
SSE	Scenario-based margin	Scenario-based margin	Extended set

Finally, we look at the effects of changing the algorithm parameters in Section 3.3.3.

3.3.1. Binary vs. Continuous Variables v. We first consider the (*LDV*) model optimized with and evaluated in the nominal scenario only (INO). The relaxation of the (*LDV*) model for the nominal case results in a large reduction in solution times without a significant compromise in plan quality (Table 8). Note that for patient 1 the dose requirement $D_{0.1cc}$ is slightly violated, though the violation is small and clinically irrelevant. The solution times of the robust model without the relaxation of v_i and the proposed algorithm from Figure 3 are unacceptable: After 5 hours, the optimality gaps remained at approximately 5%, 15%, and 10% for patients 1, 2, and 3, respectively. This makes the model with binary variables unusable and the relaxation necessary.

3.3.2. Comparison of the Treatment Plan Optimization Approaches. Treatment plans were generated for each patient using the 10 models from Table 6 where the solution times of the margin and the robust models were reduced using the algorithm in Figure 3. The nominal model was solved to optimality without using the algorithm

Treatment plan quality in terms of DVH parameters. We are interested in the distribution of the CTV and rectum DVH parameters over the scenarios. In Figure 7 we show the cumulative distribution of $D_{90\%}(CTV)$, $V_{100\%}(CTV)$, $V_{150\%}(CTV)$, $V_{200\%}(CTV)$, $D_{10\%}(Rectum)$, and $D_{2cc}(Rectum)$ for patient 1. Similar figures for patients 2–6 are provided in Section 3.1 of the online supplement (Figures 1–5). For example, in Figure 7(c)

we see that for the plan generated for patient 1 using the INO approach (solid black curve), approximately 20% of the scenarios had a $V_{150\%}(CTV)$ of 0.45 or lower. The gray area denotes values below the desired minimum value for $D_{90\%}(PTV)$ and $V_{100\%}(PTV)$, and above the desired maximum value for the remaining DVH parameters. For completeness, Table 2 in Section 3.2 of the online supplement shows the DVH parameters for the urethra. This table shows that the constraint $D_{10\%}(Urethra)$ is always satisfied.

Recall that our aim is to achieve high $D_{90\%}(CTV)$ and $V_{100\%}(CTV)$, where we aim to achieve minimum levels of 1.00 and 0.90, respectively. A curve is thus superior to another curve if it lies further to the right; our preference would be a curve that lies completely to the right of the minimum level. Similarly, for $V_{150\%}(CTV)$, $V_{200\%}(CTV)$, $D_{10\%}(Rectum)$, and $D_{2cc}(Rectum)$ curves that lie further to the left are superior, as we prefer these parameters to be small.

We first consider the models for which rectum uncertainties are unaccounted. When comparing RNO and RNE to INO and INE, respectively, we observe a shift of the complete curve of $V_{100\%}(CTV)$ toward the higher values in almost all cases. Exceptions are RNO for patient 2, which performs better than INO for the worst 15% but worse for the remaining 85% of the simulated delineations; RNE for patient 6, which performs better than INE for the worst 10% but worse for the remaining 90% of the simulations; and RNE for patient 1, where the curve lies slightly more toward the lower values than the curve corresponding to INE. Except for patient 2, SNO and SNE always yield better $V_{100\%}(CTV)$ than INO and INE, respectively. The scenario-based

Table 7. Optimality Gaps (g_2 in the Algorithm) Used for the Individual Patients

	Patient 1	Patient 2	Patient 3	Patient 4	Patient 5	Patient 6
Gap (%) robust models	0.400	0.150	0.025	0.400	0.100	0.200
Gap (%) margin models	0.400	1.000	0.025	0.400	0.100	0.200

Note. The robust approach comprises models RNO, RRO, RNE, and RRE, and the scenario-based margin approach comprises models SNO, SSO, SNE, and SSE.

Table 8. Comparison of Treatment Plans Generated with (LDV) (Without Relaxation) and Plans Generated with a Relaxation of (LDV)

DVH parameter	Unit	Patient 1		Patient 2		Patient 3	
		(LDV)	Relaxation	(LDV)	Relaxation	(LDV)	Relaxation
$D_{90\%}(PTV) \geq 1.00$	%	1.13	1.15	1.07	1.07	1.05	1.05
$V_{100\%}(PTV) \geq 0.90$	%	0.99	1.00	0.97	0.97	0.97	0.97
$V_{150\%}(PTV) \leq 0.55$	%	0.50	0.51	0.25	0.29	0.26	0.27
$V_{200\%}(PTV) \leq 0.20$	%	0.20	0.26	0.09	0.13	0.10	0.11
$D_{10\%}(Rectum) \leq 7.2$	Gy	6.8	7.3	7.2	7.2	6.9	7.0
$D_{2cc\%}(Rectum) \leq 6.7$	Gy	5.8	6.3	6.2	6.2	6.0	6.1
$D_{10\%}(Urethra) \leq 10$	Gy	9.8	10.0	9.8	9.7	9.5	9.7
$D_{0.1cc\%}(Urethra) \leq 10$	Gy	10.0	10.2	10.0	9.9	9.7	9.8
Solution time	s	14	8	385	26	25	14

DVH parameter	Unit	Patient 4		Patient 5		Patient 6	
		(LDV)	Relaxation	(LDV)	Relaxation	(LDV)	Relaxation
$D_{90\%}(PTV) \geq 1.00$	%	1.13	1.13	1.12	1.14	1.14	1.16
$V_{100\%}(PTV) \geq 0.90$	%	0.98	0.98	0.98	0.98	0.99	0.99
$V_{150\%}(PTV) \leq 0.55$	%	0.47	0.49	0.42	0.45	0.50	0.50
$V_{200\%}(PTV) \leq 0.20$	%	0.26	0.29	0.19	0.22	0.26	0.24
$D_{10\%}(Rectum) \leq 7.2$	Gy	5.5	5.6	5.2	5.2	5.6	5.8
$D_{2cc\%}(Rectum) \leq 6.7$	Gy	5.5	5.6	5.2	5.2	5.3	5.5
$D_{10\%}(Urethra) \leq 10$	Gy	9.8	10.0	9.8	9.8	9.7	9.9
$D_{0.1cc\%}(Urethra) \leq 10$	Gy	9.7	9.9	9.8	9.8	6.5	6.4
Solution time	s	2,302	498	116	10	35	9

margin and the robust optimization approach perform equally well in terms of target coverage.

Including rectum delineation inaccuracies in the optimization process, i.e., using the RR and SS models instead of the RN and SN models, respectively, yields a lower rectum dose for patients 1, 2, and 3. For patients 2 and 3 this also implies reduced target coverage. Including rectum delineation uncertainties does not affect treatment plans for patients 4, 5, and 6, as the rectum dose is already sufficiently low for these three patients: The constraint on the rectum dose was never active.

The use of a scenario-based CTV-to-PTV margin in the SN and SS models often yields an overdose to the target volume in terms of $V_{200\%}(CTV)$ compared to RN and RR. This is clear from the shift of the corresponding curves toward the right for patients 1, 4, 5, and 6. This shift is not visible for patients 2 and 3, though $V_{200\%}(CTV)$ never exceeds the maximum allowed value of 0.2 for these two patients and thus was never an active constraint. The risk of an overdose is much lower for the RN and RR models.

When comparing the use of an extended set of dwell positions to using the original set for the same model (e.g., compare INO to INE or RRO to RRE), in almost all cases the extended set allows for a reduction in $V_{150\%}(CTV)$ and $V_{200\%}(CTV)$ with little or no compromise on $V_{100\%}(CTV)$. It does, however, often yield an increased rectum dose.

Solution times. The solution times of all methods for all patients are reported in Table 9. The solution times

for RN, RR, SN, and SS approaches are still clinically acceptable due to the choice of the accepted optimality gaps. Note that the solution times of RR and SS, i.e., those models where rectum delineations are accounted for, are always the same.

**3.3.3. Changing the Algorithm's Input Parameters.** Several parameters that form an input to the optimization algorithm can affect the algorithm's performance in terms of objective value, plan quality, and solution time. In this section, we examine the effects of changing the accepted optimality gaps and the sizes of the volume fractions to be removed from the sets of calculation points.

Optimality gaps g_1 and g_2. The algorithm optimizes an instance at each iteration until the optimality gap g_1 is achieved. After all stopping criteria have been satisfied (see Figure 3), the catheter positions are fixed and the dwell times are further optimized where in each iteration an instance is optimized up to optimality gap $g_2 < g_1$.

To see the effects of choosing a different optimality gap, we optimized RNO for various values of g_2 for patients 1 and 3. We have evaluated the optimizations in terms of solution time, objective function value, and worst case $V_{100\%}(CTV)$ for the set of scenarios included in the optimization as well as the simulated scenarios used in our assessment of plan quality. Detailed results are shown in Table 3 in Section 4 of the online supplement. We did not consider gaps smaller

Figure 7. DVH Metrics for Patient 1 Obtained with Various Models and Evaluated in the Evaluation Data Set
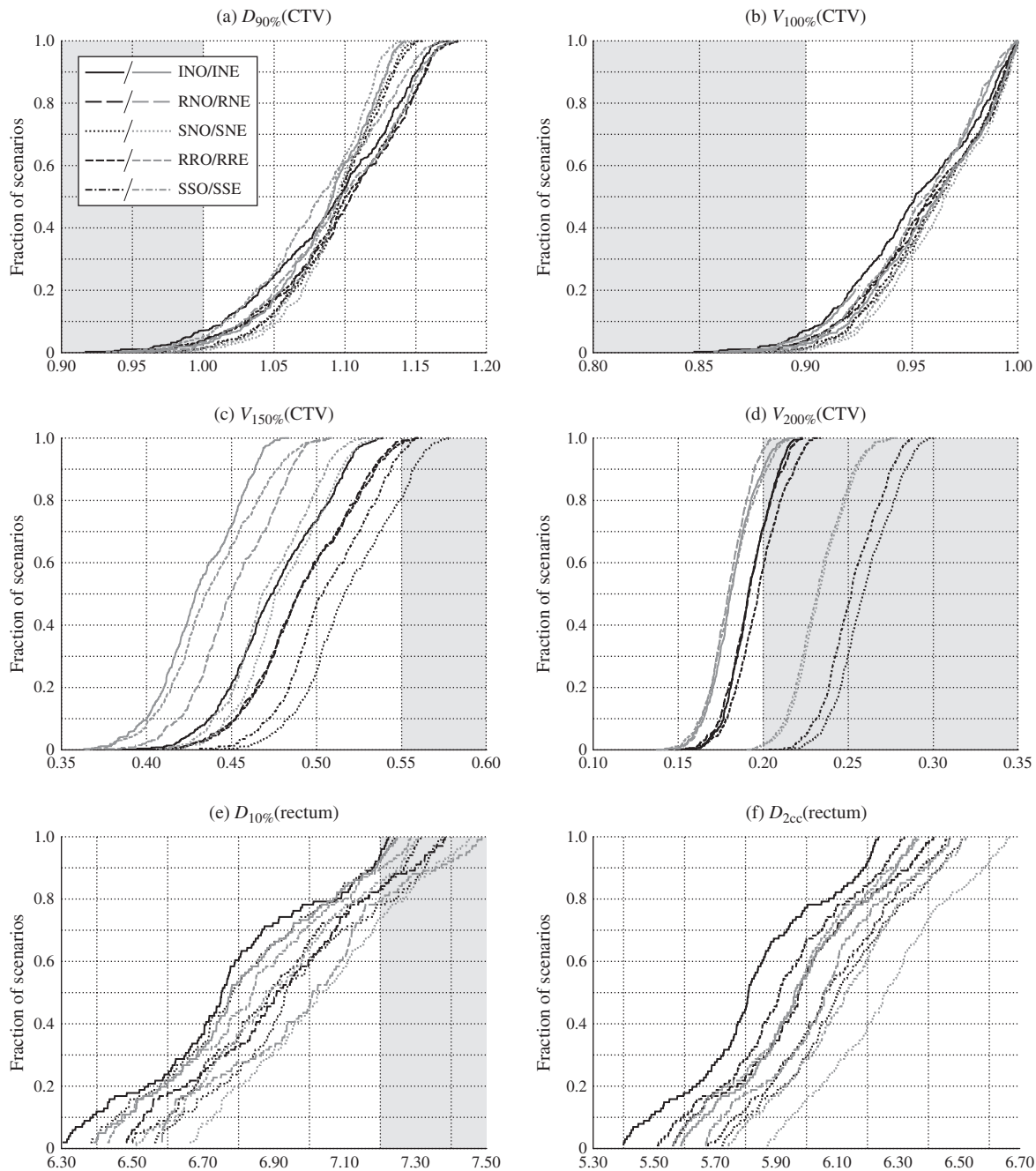
Note. The gray area indicates scenarios where the DVH requirement from Table 1 was not met.

than 0.025%, as this is already very small. Optimizing RNO for patient 1 for $g_2 = 0.3\%$ took more than three hours, so the model was not optimized for gaps smaller than 0.3%. Optimizing up to a g_2 smaller than 0.4% yields clinically unacceptable solution times for patient 1. However, setting $g_2 = 0.4\%$ gives a much lower worst case $V_{100\%}(CTV)$ than with $g_2 = 0.025\%$ for patient 3, i.e., 87.8 versus 92.7. It is thus necessary to individually determine a suitable g_2 for each patient.

Fractions of calculation points $\eta_{100\%}$ ***and*** $\eta_{200\%}$***.*** The model is optimized for subsets of the calculation points at each iteration. The algorithm also checks, per iteration, if the worst case $V_{100\%}(CTV)$ and $V_{200\%}(CTV)$ obtained for the optimized instance are sufficiently close to the real values. If this is not the case, then the sets of calculation points are extended. Recall that the parameters $\eta_{100\%}$ and $\eta_{200\%}$ determine the fractions of $\tilde{I}_C$ that are removed from $\tilde{I}_C^n$ and $\tilde{I}_C^f$, respectively. To see the

Table 9. Solution Times in Seconds

	Patient 1	Patient 2	Patient 3	Patient 4	Patient 5	Patient 6
INO	14	385	25	2,302	116	35
RNO	571	98	183	912	220	528
RRO	65	313	256	344	493	496
SNO	880	123	213	612	844	362
SSO	63	313	260	335	481	496
INE	20	439	31	804	83	12
RNE	325	218	351	53	75	150
RRE	41	88	101	75	348	365
SNE	399	87	324	52	83	144
SSE	41	87	101	74	347	366

effect of the choices for these parameters, we have optimized RNO for patient 1 for various values of $\eta_{100\%}$ and $\eta_{200\%}$. The results presented in Table 4 in Section 4 of the online supplement show that the choice of $\eta_{100\%}$ and $\eta_{200\%}$ hardly influences the objective function value and the worst case $V_{100\%}(\text{CTV})$, but they significantly influence the solution times. There is, however, no clear relation between the choice of η and the solution times. This can be explained by the trade-off that one makes when choosing η: A small η results in adding few calculation points to the optimization problem in the next iteration, which makes the optimization fast but could result in the need for more iterations. By contrast, a large η adds many calculation points to the optimization in each iteration, hence slowing the optimization but reducing the number of required iterations.

4. Discussion

Our results indicate that target coverage is improved by using the scenario-based margin model instead of the isotropic 2 mm CTV-to-PTV margin, which implies that the 2 mm margin used in the clinic may be insufficient. This particularly holds for the anterior and posterior directions of the CTV, where the delineation uncertainty is larger than in other directions (Smith et al. 2007). We conclude that an isotropic margin is inadequate. A downside of the scenario-based margin model is an increased $V_{200\%}(\text{CTV})$, which agrees with the findings from Tanderup et al. (2010). The robust treatment planning model results in an improvement in target coverage similar to the scenario-based margin approach. Additionally, in this model an overdosage, reflected in excessively high values for $V_{200\%}(\text{CTV})$, can be prevented by adding a constraint that requires $V_{200\%}(\text{CTV})$ to be below a preset level for each of the scenarios. This constraint does not work well for the margin approach, since in that case no individual scenarios are considered; thus, the constraint on $V_{200\%}(\text{CTV})$ applies to an extended CTV only, which is a rather large volume. As a result, individual scenarios were not protected from overdosage.

The dose escalation in the CTV may be caused by the absence of dwell positions in the margin volume. Therefore, we optimized a treatment plan with the scenario-based margin approach using additional dwell positions in the scenario-based margin. As this did not improve the treatment plan quality, we conclude that dose escalation inherent to the margin approach cannot be prevented by including more dwell positions.

Uncertainties in the delineation of the rectum yield risk of a rectal overdose for some patients. Our results substantiate this outcome: For those patients, accounting for rectum delineation uncertainties reduces this risk. For two out of three patients for whom this risk was reduced, this comes at a cost of a reduced coverage of the target volume.

The solution time and the optimality gap vary strongly among patients. Note that solution times vary for the nominal model as well. Furthermore, the solution time of the robust model halves for patient 1 when adding dwell positions, whereas it doubles for patient 2. These discrepancies may be caused by how much "luck" we had with the branch-and-bound tree (which also holds for the nominal optimization model). The iterative nature of our approach introduces an additional factor of "luck" in the search for an optimal solution: For one case, the procedure chose the most important scenario early, whereas more iterations were needed in another case.

For patients 1, 2, and 3 images were acquired using transrectal ultrasound imaging, whereas CT images were acquired for patients 4, 5, and 6. This results in a different delineation of the rectum: With transrectal ultrasound only the anterior wall is delineated, while the whole rectum is delineated on CT images. As a result, the rectum volumes for patients 4, 5, and 6 are approximately twice as large as for patients 1, 2, and 3. This implies that the constraint on rectum dose, $D_{10\%}(\text{Rectum}) \leq 7.2$ Gy, is less restrictive for the CT patients than for the ultrasound patients. This is inherent when using a restriction on a structure's relative volume. For our study, however, it has an advantage: The results show that including rectum delineation uncertainty yields a reduction in target coverage when $D_{10\%}(\text{Rectum})$ was above 7.2 Gy for a large subset of the scenarios, whereas target coverage is unaffected when $D_{10\%}(\text{Rectum}) \leq 7.2$ Gy was satisfied for most of the scenarios.

Our approach may be applicable for other body sites but would require reliable data on target volume and OAR delineation uncertainties of the particular organ(s) in question. Furthermore, one may apply our method to set-up uncertainties by viewing these variations as a rigid shift of the organs and hence the delineations, leaving the position of the calculation points and hence the dose rate fixed. This would allow us

to combine all uncertainties into one composite uncertainty in the index set. A thorough investigation is mandatory to assess the feasibility and value of this approach. Moreover, this approach can be used not only for HDR Brachytherapy but also for external beam radiotherapy.

The core idea of this paper on how to address uncertainties in index sets could also be applicable to other Operations Research (OR) problems. A first type of optimization model has uncertainty in the time index. For instance, supply chain models often have uncertainty in the lead time. In the food supply chain model for the UN World Food Program (Peters et al. 2016), for example, there is much uncertainty in the lead time because of possible congestion in the harbors. Optimization models with different sets of restrictions for different types of customers, regions, parts, etc., are other possibilities. An example could be inventory models with different categories of service levels, depending on customers' characteristics, and where there is uncertainty about the required service level category for a subset of future customers. Another example is optimizing flood protection measures for the coming centuries such that all safety levels are satisfied (Postek et al. 2018).

5. Conclusion

The worst-case robust treatment plan optimization model presented in this work for prostate HDR BT is capable of accounting for target volume and rectum delineation uncertainties. Uncertainties in index sets can be accounted for using a scenario-based approach. Although the treatment plan optimization model becomes too large to be solved within a clinically acceptable amount of time, our heuristic approach reduces the calculation times to acceptable proportions for the nominal and the robust optimization models.

References

Balvert M, Gorissen B, den Hertog D, Hoffmann A (2015) Dwell time modulation restrictions do not necessarily improve treatment plan quality for prostate HDR brachytherapy. *Phys. Medicine Biol.* 60(2):537–548.

Ben-Tal A, El Ghaoui L, Nemirovski A (2009) *Robust Optimization.* Princeton Series in Applied Mathematics (Princeton University Press, Princeton, NJ).

Bienstock D, Özbay N (2008) Computing robust basestock levels. *Discrete Optim.* 5(2):389–414.

Bohoslavsky R, Witte M, Janssen T, van Herk M (2013) Probabilistic objective functions for margin-less IMRT planning. *Phys. Medicine Biol.* 58(11):3563–3580.

Bortfeld T, Chan T, Trofimov A, Tsitsiklis J (2008) Robust management of motion uncertainty in intensity-modulated radiation therapy. *Oper. Res.* 56(6):1461–1473.

Chan T, Bortfeld T, Tsitsiklis J (2006) A robust approach to IMRT optimization. *Phys. Medicine Biol.* 51(10):2567–2583.

Chen W, Unkelbach J, Trofimov A, Madden T, Kooy H, Bortfeld T, Craft D (2011) Including robustness in multi-criteria opimization for intensity modulated proton therapy. *Phys. Medicine Biol.* 57(3):591–608.

Chu M, Zinchenko Y, Henderson S, Sharpe M (2005) Robust optimization for intensity modulated radiation therapy treatment planning under uncertainty. *Phys. Medicine Biol.* 50(23):5463–5477.

De Boeck L, Beliën J, Egyed W (2014) Dose optimization in high-dose-rate brachytherapy: A literature review of quantitative models from 1990–2010. *Oper. Res. Health Care* 3(2):80–90.

De Brabandere M, Hoskin P, Haustermans K, Van den Heuvel F, Siebert FA (2012) Prostate post-implant dosimetry: Interobserver variability in seed localisation, contouring and fusion. *Radiotherapy Oncology* 104(2):192–198.

Deist TM, Gorissen BL (2016) High-dose-rate prostate brachytherapy inverse planning on dose-volume criteria by simulated annealing. *Phys. Medicine Biol.* 61(3):1155–1170.

Fredriksson A (2012) A characterization of robust radiation therapy treatment planning methods—From expected value to worst case optimization. *Medical Phys.* 39(8):5169–5181.

Fredriksson A (2013) Robust optimization of radiation therapy accounting for geometric uncertainty. Unpublished doctoral dissertation, KTH Engineering Sciences, Stockholm, Sweden.

Fredriksson A, Bokrantz R (2014) A critical evaluation of worst case optimization methods for robust intensity-modulated proton therapy planning. *Medical Phys.* 41(8):081701.

Fredriksson A, Forsgren A, Hårdemark B (2011) Minimax optimization for handling range and setup uncertainties in proton therapy. *Medical Phys.* 38(3):1672–1684.

Gorissen B, den Hertog D, Hoffmann A (2013) Mixed integer programming improves comprehensibility and plan quality in inverse optimization of prostate HDR brachytherapy. *Phys. Medicine Biol.* 58(4):1041–1057.

Granero D, Pérez-Calatayud J, Casal E, Ballester F, Venselaar J (2006) A dosimetric study on the Ir-192 high dose rate Flexisource. *Medical Phys.* 33(12):4578–4582.

Holm A, Larsson T, Tedgren A (2013) A linear programming model for optimizing HDR brachytherapy dose distributions with respect to the mean dose in the DVH-tail. *Medical Phys.* 40(8):081705.

Hoskin P, Motohashi K, Bownes P, Bryant L, Ostler P (2007) High dose rate brachytherapy in combination with external beam radiotherapy in the radical treatment of prostate cancer: Initial results of a randomised phase three trial. *Radiotherapy Oncology* 84(2):114–120.

Hoskin P, Colombo A, Henry A, Niehoff P, Hellebust TP, Siebert F, Kovacs G (2013) GEC/ESTRO recommendations on high dose rate afterloading brachytherapy for localised prostate cancer: An update. *Radiotherapy Oncology* 107(3):325–332.

International Commission on Radiation Units and Measurements (1999) *ICRU* 62. *Prescribing, Recording and Reporting Photon Beam Therapy* (Oxford University Press, Oxford, UK).

Kirisits C, Rivard M, Baltas D, Ballester F, De Brabandere M, Van der Laarse R, Niatsetski Y, Papagiannis P, Hellebust T, Perez-Calatayud J, Tanderup K, Venselaar J, Siebert F (2014) Review of clinical brachytherapy uncertainties: Analysis guidelines of GEC-ESTRO and the AAPM. *Radiotherapy Oncology* 110(1):199–212.

Lessard E, Pouliot J (2001) Inverse planning anatomy-based dose optimization for HDR-brachytherapy of the prostate using fast simulated annealing algorithm and dedicated objective function. *Medical Phys.* 28(5):773–779.

Liu W, Zhang X, Li Y, Mohan R (2012) Robust optimization of intensity modulated proton therapy. *Medical Phys.* 39(2):1079–1091.

Nath R, Anderson L, Luxton G, Weaver K, Williamson J, Meigooni A (1995) Dosimetry of interstitial brachytherapy sources: Recommendations of the AAPM radiation therapy committee task group no. 43. *Medical Phys.* 22(2):209–234.

Olafsson A, Wright S (2006) Efficient schemes for robust IMRT treatment planning. *Phys. Medicine Biol.* 51(21):5621–5642.

Peters K, Fleuren H, den Hertog D, Kavelj M, Silva S, Goncalves R, Ergun O, Soldner M (2016) The nutritious supply chain: Optimizing humanitarian food aid. CentER Discussion Paper, Center for Economic Research, Tilburg University, Tilburg, Netherlands.

Postek K, den Hertog D, Kind J, Pustjens C (2018) Adjustable robust strategies for flood protection. *Omega* 82(January):142–154.

Rylander S, Buus S, Pedersen EM, Bentzen L, Tanderup K (2017) Dosimetric impact of contouring and needle reconstruction uncertainties in US-, CT- and MRI-based high-dose-rate prostate brachytherapy treatment planning. *Radiotherapy* 123(1):125–132.

Siauw T, Cunha A, Atamtürk A, Hsu I, Pouliot J, Goldberg K (2011) IPIP: A new approach to inverse planning for HDR brachytherapy by directly optimizing dosimetric indices. *Medical Phys.* 38(7):4045–4051.

Smith W, Lewis C, Bauman G, Rodrigues G, D'Souza D, Ash R, Ho D, Venkatesan V, Downey D, Fenster A (2007) Prostate volume contouring: A 3D analysis of segmentation using 3DTRUS, CT and MR. *Internat. J. Radiation Oncology* 67(4):1238–1247.

Tanderup K, Pötter R, Lindegaard J, Berger D, Wambersie A, Kirisits C (2010) PTV margins should not be used to compensate for uncertainties in 3D image guided intracavitary brachytherapy. *Radiotherapy Oncology* 97(3):495–500.

Unkelbach J, Ulfke U (2004) Inclusion of organ movements in IMRT treatment planning via inverse planning based on probability distributions. *Phys. Medicine Biol.* 49(17):4005–4029.

Van Herk M (2004) Errors and margins in radiotherapy. *Seminars Radiation Oncology* 14(1):52–64.

Van Herk M, Remeijer P, Lebesque JV (2002) Inclusion of geometric uncertainties in treatment plan evaluation. *Internat. J. Radiation Oncology Biol. Phys.* 52(5):1407–1422.

Villeirs GM, Van Vaerenbergh K, Vakaet L, Bral S, Claus F, De Neve WJ, Verstraete KL, De Meerleer GO (2005) Interobserver delineation variation using CT versus combined CT + MRI in intensity-modulated radiotherapy for prostate cancer. *Strahlentherapie Onkologie* 181(7):424–430.

Weiss E, Hess C (2003) The impact of gross tumor volume (GTV) and clinical target volume (CTV) definition on the total accuracy in radiotherapy theoretical aspects and practical experiences. *Strahlentherapie Onkologie* 179(1):21–30.

Yamada Y, Rogers L, Demanes D, Morton G, Prestidge B, Pouliot J, Cohen G, Zaider M, Ghilezan M, Hsu I (2012) American brachytherapy society consensus guidelines for high-dose-rate prostate brachytherapy. *Brachytherapy* 11(1):20–32.